Materials Research. 2022; 25:e20220312
DOI: https://doi.org/10.1590/1980-5373-MR-2022-0312

The Effect of EDTA Functionalization on Fe_3O_4 Thermal Behavior

Daniel B. Fumis[a], Maria L.D.C Silveira[a], Caroline Gaglieri[a], Laura T. Ferreira[b], Rodrigo F.C. Marques[b], Aroldo G. Magdalena[a]*

[a]Universidade Estadual Paulista, Faculdade de Ciência, Departamento de Química, Bauru, SP, Brasil.
[b]Universidade Estadual Paulista, Departamento de Química Analítica, Físico-Química e Inorgânica do Instituto de Química, Araraquara, SP, Brasil.

Received: July 11, 2022; Revised: September 21, 2022; Accepted: October 6, 2022

The surface of Fe_3O_4 nanoparticles is very reactive and can oxidize to γ-Fe_2O_3 (maghemite) and α-Fe_2O_3 (hematite) structures. Based on this, the oxidation process of Fe_3O_4 nanoparticles must be prevented, and one of the strategies is surface functionalization with organic or inorganic molecules. Thus, this study analyzed the thermal behavior of Fe_3O_4 and Fe_3O_4-EDTA nanoparticles using X-ray diffraction (XRD), simultaneous thermogravimetry-differential thermal analysis (TG-DTA), differential scanning calorimetry (DSC). Results showed that γ- Fe_2O_3 was obtained as an intermediate in Fe_3O_4 and Fe_3O_4-EDTA decomposition, as confirmed by TG-DTA and DSC curves. Moreover, Fe_3O_4-EDTA exhibited a temperature peak (T_p = 573.5°C) of phase transformation (γ-Fe_2O_3 → α-Fe_2O_3) higher than that of Fe_3O_4 (T_p = 533.0°C), confirming that EDTA molecules stabilized the nanoparticles efficiently. The kinetic behavior of samples changed, and the activation energy for functionalized samples decreased.

Keywords: *Magnetite, Maghemite, Hematite, Non-isothermal kinetics.*

1. Introduction

Magnetite (Fe_3O_4) is an oxide formed by Fe^{3+} and Fe^{2+} ions in a 2:1 molar ratio, in the pH range between 9 and 14, and preferably in the absence of oxygen[1,2]. Its unit cell is based on a cubic system (face-centered cubic), which provides different O^{2-} ion coordination according to the type of interstitial: in the octahedral, the anions to both iron ions (Fe^{2+} and Fe^{3+}) are coordinated; while in the tetrahedral, only Fe^{3+} is coordinated[3]. The Fe^{3+} ions are equally distributed in octahedral and tetrahedral interstices, while all Fe^{2+} ions only occur in octahedral interstices. Hence, the magnetic behavior of Fe_3O_4 is associated with this ion[4-6]. Considering their position in the crystalline structure, Fe^{2+} ions can easily oxidize to Fe^{3+}[5,7]. Consequently, the co-precipitation must be synthesized under an inert atmosphere (nitrogen or argon) to prevent the oxidation of Fe^{2+} to Fe^{3+}. The main crystalline phases of iron oxide are magnetite (Fe_3O_4), maghemite (γ- Fe_2O_3), and hematite (α- Fe_2O_3). The first and second phases show similar properties, but α- Fe_2O_3 exhibits distinct characteristics from the others[3,7-10]. Currently, Fe_3O_4 nanoparticles have received increasing attention due to their simple syntheses and stable storage in the colloidal form[7,11]. Nevertheless, the agglomeration of nanoparticles is expected over time to reduce the surface energy provided by the large surface area of nanoparticles[1,12-14]. Moreover, the oxidation process reduces magnetic properties. Based on this, strategies must be developed to provide colloidal protection and chemistry stabilization for Fe_3O_4 nanoparticles. For instance, there are already nanoparticles covered with organic (alkoxysilanes, proteins, etc)[15] or inorganic (metal oxides, metals, etc) species[16]. The surface functionalization of nanoparticles can introduce new functions to nanoparticles, as it can change the chemical and physical properties. In the case of Fe_3O_4 nanoparticles, it appears that the functionalization can improve the colloidal stability[1,2,17-23], increase the chemical and thermal stability against the oxidation reaction[23], but depending on the functionalizing agent it can decrease the magnetic property[24-26] The oxidation reaction of the Fe_3O_4 nanoparticles is one of the factors that contributes to the decrease in the magnetic properties. In addition to these functions mentioned above, Marcos-Hernández et al.[27] studied nano-Fe_3O_4 electrodes with the aim of electrochemical reduction of nitrate. This expands the application possibilities of functionalized nanoparticles.

Temperature changes can promote several chemical and physical processes in nanoparticles. Under heating, Fe_3O_4 converts to other oxides, following the reaction sequence showed in reaction (1)[3,9-11]:

$$2Fe_3O_4 + \tfrac{1}{2}O_2 \rightarrow 3\gamma - Fe_2O_3 \rightarrow 3\alpha - Fe_2O_3 \text{ Reaction} \quad (1)$$

Hence, a thermal study with simultaneous thermogravimetry-differential thermal analysis (TG-DTA) and differential scanning calorimetry (DSC) associated with X-ray powder diffraction (XRPD) can provide information about the influence of functionalization on the oxidation of Fe_3O_4. Functionalization is not expected to change the reaction sequence but only modify the mechanism and stabilize the crystalline phase. Non-isothermal kinetics could investigate the modification in the reaction mechanism, as data are obtained *in situ*, which is considered an advantage and, therefore, has been applied to several materials[28-42]. Thus, this study aims

*e-mail: aroldo.magdalena@unesp.br

to investigate the influence of EDTA functionalization on thermal behavior and the sequence of reactions observed when heating Fe_3O_4 nanoparticles.

2. Materials and Methods

2.1. Chemicals

The reagents used for the synthesis were iron (II) chloride tetrahydrate (Merck), iron (III) chloride hexahydrate (Sigma Aldrich), ammonium hydroxide ~ 28% (Synth), acetone P.A. (Synth), and Ethylenediaminetetraacetic acid- EDTA (99%) (Synth).

2.1. Synthesis and modification of Fe_3O_4

The nanoparticle syntheses were reported in a previous study[23]. Quantities of 0.03 mol of iron (III) chloride hexahydrate and 0.015 mol of iron (II) chloride tetrahydrate were mixed in 100 mL of distilled water. Then, 10 mL of ammonium hydroxide was added to the system, followed by 50 mL of EDTA solution (0.002 mol L^{-1}). The mixture was stirred for 1 hour at room temperature in an inert atmosphere (nitrogen). The resulting precipitate was separated with a magnet and washed several times with distilled water. Then, the samples were dried at 60.0°C in a laboratory oven. This methodology leads to the formation of Fe_3O_4-EDTA nanoparticles. The Fe_3O_4 nanoparticles were obtained in the same way but without adding the EDTA solution.

2.2. Analytical instruments

2.2.1. Simultaneous thermogravimetry-differential thermal analysis (TG-DTA) and differential scanning calorimetry (DSC)

The TG-DTA curves were obtained with a thermal analysis system from Netzsch, model STA 449 F3. Approximately 5 mg of the sample was measured and placed in an open crucible of 200.0 µL of α-alumina. A dry air atmosphere was used, with a flow rate of 70.0 mL min^{-1}, and the temperature ranged between 30-800°C. The heating rate was 10.0°C min^{-1}.

The DSC was analyzed on a Mettler-Toledo equipment, model DSC 1 Star^e System. The sample mass was approximately 4 mg, placed in an open crucible of 40.0 µL of α-alumina, with flow and heating rates of 50.0 mL min^{-1} and 10.0°C min^{-1}, respectively. The experiment was performed under air and nitrogen atmospheres. Under air, the temperature ranged from 25°C to 300°C, while under nitrogen, the sample was heated from 25.0-150.0°C for 5 minutes (to eliminate the residual water in the sample), then cooled to 0°C, and heated to 400.0°C. It is worth noting that before this experiment, Fe_3O_4 was heated to 140.0°C to eliminate the water.

2.2.2. X-ray powder diffraction (XRPD)

The X-ray powder diffraction was measured in a Rikagu, model MiniFlex 600, using Cu Kα radiation (λ = 1.54056Å) and settings of 40 kV and 20 mA in the 2θ range of 10 to 80°, 10° min^{-1}.

2.2.3. Kinetic parameters

Non-isothermal kinetics was analyzed following the ICTAC recommendations[43]. The curves with different heating rates (5.0, 10.0, 15.0, and 20.0°C min^{-1}) were obtained in the same equipment and experimental conditions as the previous topic in a dry air atmosphere. The data were processed with the NETZSCH kinetics Neo Trial software by Netzsch[44]. The Friedman model-free method was used[45], a derivative method that is more sensitive than integrative ones[35]. Its expression is shown in Equation 1:

$$ln[\beta_i(\frac{d\alpha}{dT})_{\alpha,i}] = ln\left[f(\alpha)A_\alpha\right] - \frac{E_\alpha}{RT_{\alpha,i}} \qquad \text{Equation (1)}$$

where β_i is the heating rate (°C min^{-1}), R is the gas constant (8.3145 J K^{-1} mol^{-1}), and A_α (the unit of the lnA_α is cm^3 mol^{-1} s^{-1}) and E_α (kJ mol^{-1}) parameters are the pre-exponential factor and activation energy, respectively.

3. Results and Discussion

3.1. Thermogravimetry-differential thermal analysis (TG-DTA) and differential scanning calorimetry (DSC)

Figure 1 shows TG-DTA curves. The TG curve of Fe_3O_4 (Figure 1a) shows a mass loss between 30.0 and 120.4°C (Δm = 1.86%), which refers to the water evaporation of the sample. After this thermal event, there was a small mass increase (Δm = 0.54%) in the TG curve between 160.0 and 288.9°C, and this value did not change up to 800°C.

Some studies in the literature have reported that, under air atmosphere, γ- Fe_2O_3 is obtained as an intermediate in Fe_3O_4 thermal decomposition[32,36,46], which causes a mass gain in the TG curve. This change in sample mass is resulted from oxygen (O_2) incorporation and has been well described

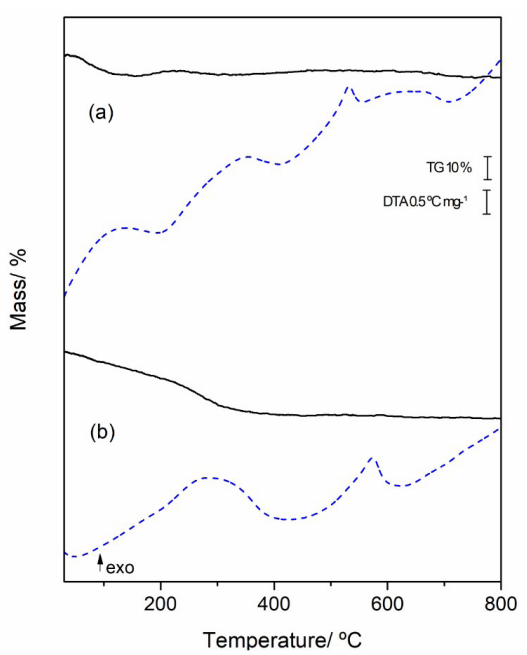

Figure 1. TG/DTA curves of Fe_3O_4 *(a)* and Fe_3O_4-EDTA *(b)*.

by Sanders and Gallager[32], in which they have suggested a complex process for Fe_3O_4 thermal decomposition into a-Fe_2O_3 based in the global reaction (2):

$$2Fe_3O_4 + O_2 \rightarrow X \rightarrow Y \rightarrow 3\,a-Fe_2O_3 \text{ Reaction} \quad (2)$$

In the present reaction, X and Y species can be considered as γ- Fe_2O_3 and are intermediates of the reaction, since its consumed immediately after is formation[32]. In addition, the experimental value obtained by the authors (Δm_{exp} = + 3.47%) was very close to the theoretical value (Δm_{exp} = + 3.46%), corroborating the suggested mechanism. Nie et al.[34] monitoring the surface structure of magnetite (100) during O_2 exposure at a temperature of 650°C and the authors found no evidence of maghemite formation. The oxidation of Fe_3O_4 depends on its origin and nature[46], besides other factors such as temperature and sample size[3,47]. Considering that the mass gain observed did not result in any signal in the DTA curve, and the Δm observed is lower than the equipment error (1%), it was impossible to confirm the formation of γ- Fe_2O_3 as an intermediate of Fe_3O_4 synthesized in this study. The DSC was analyzed to confirm this event and will be discussed later. Despite the absence of any other event in the TG curve until the end of the analysis, the DTA curve showed an exothermic peak at 533.0°C, which could be associated with a formation in the α- Fe_2O_3 phase.

Figure 1b shows the TG-DTA curves of Fe_3O_4-EDTA nanoparticles. Between 30.0 and 351.2°C, there was a subtle and continuous mass loss (Δm = 5.20%) associated with water evaporation and degradation of organic matter from EDTA molecules. One of our previous studies[23] discussed the interaction between Fe_3O_4 nanoparticles and EDTA molecules, and the results showed that the Fe_3O_4 surface is binding to the carboxylates of the EDTA molecules. Based on this, it is suggested that EDTA molecules stabilize Fe_3O_4 nanoparticles[23]. As a result, the exothermic event associated with a formation in the α- Fe_2O_3 phase was dislocated in the DTA curve to a higher temperature (573.5°C) than that of non-functionalized Fe_3O_4 (533.0°C). This result corroborates the stabilization of Fe_3O_4 nanoparticles, which are less susceptible to oxidation when functionalized with EDTA and corroborate the previous result obtained by other techniques for this system[23]. In addition, it also supports the stabilization of Fe_3O_4 nanoparticles by the coprecipitation method with organic molecules, such as also observed when used chitosan[17].

The temperature overlaps of organic matter decomposition of Fe_3O_4-EDTA did not allow verifying whether there was any mass gain in the TG curve between 160.0 and 288.9°C. It is possible to affirm that the events in DTA curves are endothermic or exothermic considering the technique principle, which in a very simplified description indicates the temperature difference between the sample and a reference, which are exposed to the same controlled experimental conditions. In all DTA curves, the axis direction must be represented; as a result, in the present paper, they are exhibited as an up arrow in all DTA curves. The complete technique details can be found in specialized reference[48].

Figure 2 shows the DSC curve under the air atmosphere of Fe_3O_4. There was an endothermic event (T_p = 51.1°C and ΔH = 39.2 J g^{-1}) associated with water evaporation in magnetite. From 187.8°C, the baseline increases proportionally with the temperature, indicating a potential material change. However, there is an evident exothermic event between 247.0 and 280.1°C (T_p = 263.6°C and ΔH = 2.1 J g^{-1}). These events agree with those of the TG curve of Fe_3O_4 (Figure 1a).

Figure 3 shows the cycle of DSC curves of Fe_3O_4 under a nitrogen atmosphere to investigate this event better. The first heating procedure (Figure 3a) showed a small endothermic event between 75.7°C and 132.0°C associated with residual water evaporation. The first cooling procedure showed many

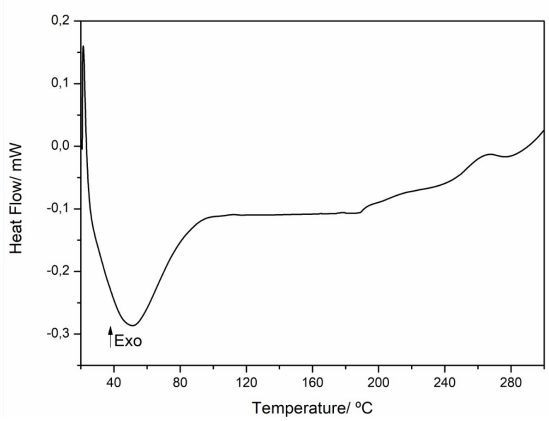

Figure 2. DSC curve of Fe_3O_4 under air atmosphere.

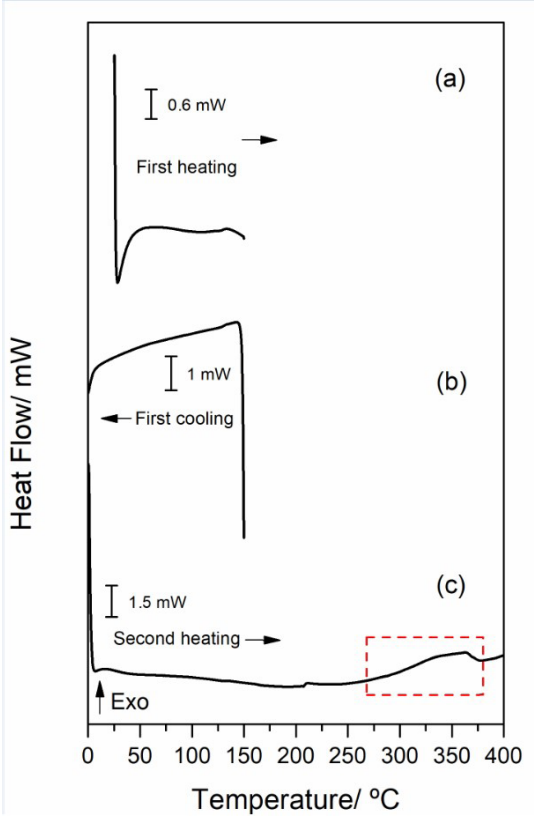

Figure 3. Cycle of DSC curves of Fe_3O_4 under nitrogen atmosphere: 0-150°C *(a)*, 150-0°C *(b)*, and 0-400°C *(c)*.

thermal events. However, the second heating procedure showed an exothermic peak (T_p = 339.7°C) with ΔH= 79.4 J g^{-1}. Under a nitrogen atmosphere, the temperature peak (T_p) was dislocated to a higher value, which could be explained by the occurring oxidation reaction: converting Fe^{2+} to Fe^{3+} in Fe_3O_4 resulting in γ- Fe_2O_3. Although the atmosphere used is considered inert, the nitrogen cylinder has a minimum amount of oxygen enough to cause the reaction under higher temperatures.

Both experiments (air and nitrogen) showed a thermal event, confirming that the Δm observed in the TG curve of Fe_3O_4 (0.54%) was a mass gain instead of a baseline deviation. Moreover, this event might have resulted from the formation of γ- Fe_2O_3. The DSC of Fe_3O_4-EDTA was not analyzed because the organic thermal degradation of the sample starts at low temperatures, which could mask other signals in the DSC curve.

3.2. X-ray powder diffraction (XRPD)

The samples of Fe_3O_4 and Fe_3O_4-EDTA were heated from room temperature to 350°C and 600°C to compare the phases obtained at each temperature. Then, the samples were analyzed with X-ray diffraction. Comparing the diffractograms of Fe_3O_4 at room temperature (Figure 4a) with Fe_3O_4 at 350°C allowed verifying a small peak around 2θ = 25° associated with the α-Fe_2O_3 structure. The α-Fe_2O_3 has a hexagonal structure seen in the curve of Figure 4c. However, the diffractogram at this temperature is similar to the structures of Fe_3O_4 and γ-Fe_2O_3 with cubic systems[3]. Thus, the DSC data suggests that Fe_3O_4 nanoparticles were oxidized to γ-Fe_2O_3, and the transformation to α-Fe_2O_3 was initiated at a peak temperature of around 533°C (Figure 1). Above this peak temperature, the α-Fe_2O_3 formation reaction was completed, as shown in the diffractogram of Figure 4c. Although the literature reports that γ- Fe_2O_3 is completely converted to α- Fe_2O_3 above 325°C, this study only showed signs of the beginning of α-Fe_2O_3 formation reaction at a temperature of 350°C.

The surface functionalization of Fe_3O_4 nanoparticles was performed in a single step and this changed the mechanism of formation of the functionalized nanoparticles, decreasing the size of the nanoparticles[23] and consequently changing the properties of their colloidal[23] and thermal properties of the nanoparticles. The diffractogram results of EDTA-functionalized nanoparticles showed the formation of α-Fe_2O_3 only at 600°C. This indicates that functionalization has protected from the oxidation reaction compared to non-functionalized nanoparticles.

3.3. Kinetic results of the formation of α-Fe_2O_3

Some studies have reported kinetic analyses on the solid-solid transition of Fe_3O_4 to γ- Fe_2O_3[32,36]. A non-isothermal kinetic study was performed to investigate better the second phenomenon (α-Fe_2O_3 formation) and the functionalization effect on phase transition. Figure 5 presents the DTA curves obtained at different heating rates for each sample. A kinetic model should provide pertinent information about the dependence between activation energy and extent of reaction, as well as determine the kinetic triplet (E_α, A_α, and reaction type).

The software allowed fitting the extent of reactions with the Friedman model-free method[42]. Figure 6 shows the graphic dependence of E_α vs. α from the formation of α-Fe_2O_3 obtained for Fe_3O_4 and Fe_3O_4-EDTA samples. For Fe_3O_4, the activation energy values were almost constant at around 149.0 kJ mol^{-1} up to α = 41.0%. Then, there was a constant decrease in activation energy values up to 82.0 kJ mol^{-1}. This profile (without shoulders or high variations in activation energy values with the increase in the extent of reaction) suggests an independent reaction (A → B)[42]. The graphic dependence profile of E_α vs. α of the Fe_3O_4-EDTA sample showed different behavior. The activation energy value begins at 234.0 kJ mol^{-1} and decreases slowly up to 224.0 kJ mol^{-1} (α = 67.0%). Hence, the value keeps decreasing up to 211.0 kJ mol^{-1}. Moreover, these values were higher than that of the non-functionalized material.

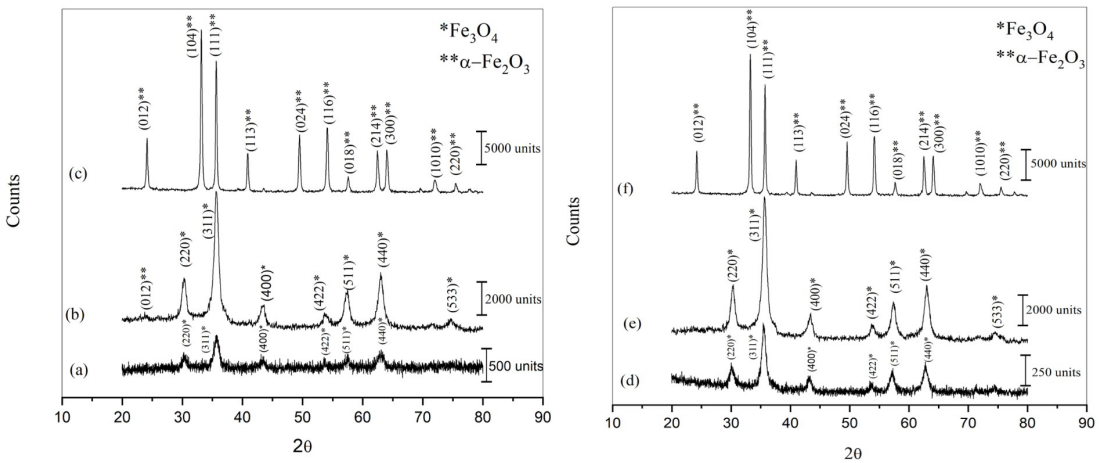

Figure 4. X-ray diffractograms of nanoparticles at different temperatures: Fe_3O_4 at room temperature (a), Fe_3O_4 at 350°C (b), Fe_3O_4 at 600°C (c), Fe_3O_4-EDTA at room temperature (d), Fe_3O_4-EDTA at 400°C (e), and Fe_3O_4-EDTA at 650°C (f). It agrees with the peak pattern from Crysmet 867299 (Fe_3O_4), Crysmet 967300 (γ- Fe_2O_3), and Crysmet 854228 (α- Fe_2O_3).

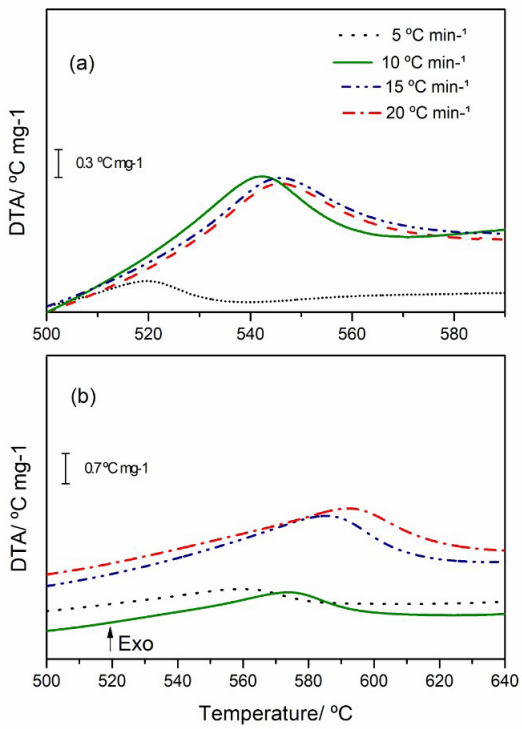

Figure 5. DTA curves at different heating rates for the formation of α- Fe_2O_3 from Fe_3O_4 *(a)* and Fe_3O_4-EDTA *(b)*.

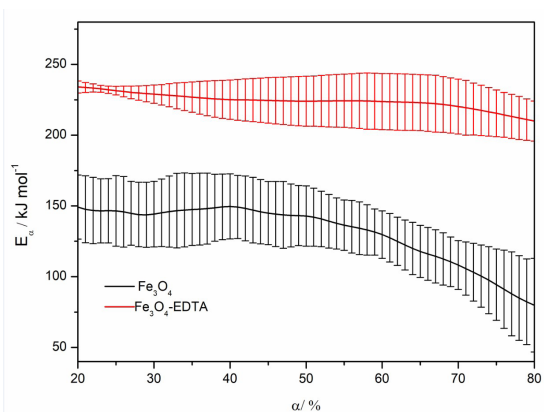

Figure 6. E_α dependence on α by non-isothermal analyses of DTA data for Fe_3O_4 and Fe_3O_4-EDTA samples using the Friedman method.

Although the value changes were small, the profile did not suggest the occurrence of independent reactions.

The transformation of γ- Fe_2O_3 into α- Fe_2O_3 requires the atomic rearrangement from a cubic to a hexagonal system. This process occurs with the diffusion of iron and oxygen atoms. However, there was a different diffusion of these atoms (Fe_3O_4 to γ- Fe_2O_3), consequently creating vacancies in the crystalline structure. Then, these vacancies were consumed in the transition of γ-Fe_2O_3 to α-Fe_2O_3[34]. The hematite nucleus previously formed catalyzed the reaction (autocatalytic), justifying the decrease in activation energy values observed in Figure 6 for the Fe_3O_4 nanoparticles.

Besides modifying the Fe-O bond by nanoparticle functionalization, the sample surface also changed[23]. Additionally, the literature shows that γ- Fe_2O_3 grows from the core to the surface of magnetite[34]. These facts corroborate the kinetic data obtained in this study, which shows a decrease in activation energy for EDTA-functionalized nanoparticles.

4. Conclusions

The γ- Fe_2O_3 was obtained as an intermediate in Fe_3O_4 and Fe_3O_4-EDTA decomposition, as confirmed by TG-DTA and DSC curves. Moreover, the Fe_3O_4-EDTA exhibited a higher temperature peak (T_p = 573.5°C) of transition (γ- Fe_2O_3 → α-Fe_2O_3) than Fe_3O_4 (T_p = 533.0°C), observed in DTA curves, confirming that EDTA molecules stabilize the nanoparticles efficiently. Then, the transformation reaction also changed, decreasing the activation energy of EDTA-functionalized nanoparticles.

5. Acknowledgements

This study was financed in part by the Coordenação de Aperfeiçoamento de Pessoal de Nível Superior – Brazil (CAPES) – Finance Code 001. The authors would like to thank CAPES (proc. 024/2012 and 011/2009 Pro-equipment), POSMAT/UNESP, FAPESP (processes: 2013/09022-7, 2015/00615-0, and 2016/01599-1), and CNPq (Processes 302267/2015-8 and 302753/2015-0) for the financial support.

6. References

1. Gupta AK, Gupta M. Synthesis and surface engineering of iron oxide nanoparticles for biomedical applications. Biomaterials. 2005;26(18):3995-4021.
2. Lu A-H, Salabas EL, Schüth F. Magnetic nanoparticles: synthesis, protection, functionalization, and application. Angew Chem Int Ed. 2007;47(8):1222-44.
3. Cornell RM, Schwertmann U. The iron oxides: structure, properties, reactions, occurrences and uses. 2nd ed. Weinheim: Wiley-VCH; 2003.
4. Samuel CN, Irene MCL. Magnetic Nanoparticles: essential factors for sustainable environmental applications. Water Res. 2012;47:2613-32.
5. Oliveira LCA, Fabris JD, Pereira NC. Óxidos de ferro e suas aplicações em processos catalíticos: uma revisão. Quim Nova. 2013;36(1):123-30.
6. Santana GP, Ramos AM, Fabris JD. Uma estratégia adaptada para a síntese de magnetita. Quim Nova. 2008;31(2):430-2.
7. Nguyen ND, Tran HV, Xu S, Lee TR. Fe_3O_4 nanoparticles: structures, synthesis, magnetic properties, surface functionalization, and emerging applications. Appl Sci. 2021;11(23):11301.
8. Maksoud MIAA, El-Sayyad GS, Abokhadra A, Soliman LI, El-Bahnasawy HH, Ashour AH. Influence of Mg^{2+} substitution on structural, optical, magnetic, and antimicrobial properties of Mn–Zn ferrite nanoparticles. J Mater Sci Mater Electron. 2020;31(3):2598-616.
9. Leonel AC, Mansur AAP, Mansur HS. Advanced functional nanostructures based on magnetic iron oxide nanomaterials for water remediation: a review. Water Res. 2021;190(15):116693.
10. Pham T, Huy TQ, Le AT. Spinel ferrite (AFe_2O_4)-based heterostructured designs for lithium-ion battery, environmental monitoring, and biomedical applications. RSC Advances. 2020;10(52):31622-61.
11. Bini RA, Marques RFC, Santos FJ, Chaker JA, Jafelicci M Jr. Synthesis and functionalization of magnetite nanoparticles

with different amino-functional alkoxysilanes. J Magn Magn Mater. 2012;324(4):534-9.
12. Veisi H, Joshani Z, Karmakar B, Tamoradi T, Heravi MM, Gholami J. Ultrasound assisted synthesis of Pd NPs decorated chitosan-starch functionalized Fe_3O_4 nanocomposite catalyst towards Suzuki-Miyaura coupling and reduction of 4-nitrophenol. Int J Biol Macromol. 2021;172:104-13.
13. Panahandeh A, Parvareh A, Moraveji MK. Synthesis and characterization of γ-MnO_2/chitosan/Fe_3O_4 cross-linked with EDTA and the study of its efficiency for the elimination of zinc (II) and lead (II) from wastewater. Environ Sci Pollut Res Int. 2021;28(8):9235-54.
14. Qin M, Xu M, Niu L, Cheng Y, Niu X, Kong J, et al. Multifunctional modification of Fe_3O_4 nanoparticles for diagnosis and treatment of diseases: a review. Front Mater Sci. 2021;15(1):36-53.
15. Saire-Saire S, Garcia-Segura S, Luyo C, Andrade LH, Alarcon H. Magnetic bio-nanocomposite catalysts of $CoFe_2O_4$/hydroxyapatite-lipase for enantioselective synthesis provide a framework for enzyme recovery and reuse. Int J Biol Macromol. 2020;148:284-91.
16. Saire-Saire S, Barbosa ECM, Garcia D, Andrade LH, Garcia-Segura S, Camargo PH, et al. Green synthesis of Au decorated $CoFe_2O_4$ nanoparticles for catalytic reduction of 4-nitrophenol and dimethylphenylsilane oxidation. RSC Advances. 2019;9(38):22116-23.
17. Silveira MLDC, Silva IMD, Magdalena AG. Synthesis and characterization of Fe_3O_4-NH_2 and Fe_3O_4-NH_2-chitosan nanoparticles. Ceramica. 2021;67(383):295-300.
18. Neves RP, Bronze-Uhle ES, Santos PL, Lisboa-Filho PN, Magdalena AG. Salicylic acid incorporation in Fe_3O_4-BSA nanoparticles for drug release. Quim Nova. 2021;44:824-9.
19. Shafiq M, Alazba A, Amin MT. Synthesis of a novel EDTA-functionalized nanocomposite of Fe_3O_4-Eucalyptus camaldulensis green carbon fiber for selective separation of lead ions from synthetic wastewater: isotherm and kinetic studies. Appl Nanosci. 2022. In press.
20. Mohammadi H, Nekobahr E, Akhtari J, Saeedi M, Akbari J, Fathi F. Synthesis and characterization of magnetite nanoparticles by co-precipitation method coated with biocompatible compounds and evaluation of in-vitro cytotoxicity. Toxicol Rep. 2021;8:331-6.
21. Rahman ZU, Kanwal S, Khan S, Qureshi MN, Al-Ghamdi YO. A facile approach to fabricate magnetic and mesoporous Fe_3O_4@Au@mTiO_2 composite. J Mater Sci Mater Electron. 2021;32(7):8837-47.
22. Salman D, Juzsakova T, Al-Mayyahi MA, Ákos R, Mohsen S, Ibrahim RI, et al. Synthesis, Surface Modification and Characterization of Magnetic Fe_3O_4@SiO_2 Core-Shell Nanoparticles. J Phys Conf Ser. 2021;1773(1):012039.
23. Magdalena AG, Silva IMB, Marques RFC, Pipi ARF, Lisboa-Filho PN, Jafelicci M Jr. EDTA-functionalized Fe_3O_4 nanoparticles. J Phys Chem Solids. 2018;113:5-10.
24. Albalawi AE, Khalaf AK, Alyousif MS, Alanazi AD, Baharvand P, Shakibaie M, et al. Fe_3O_4@piroctone olamine magnetic nanoparticles: synthesize and therapeutic potential in cutaneous leishmaniasis. Biomed Pharmacother. 2021;139:111566.
25. Nigam B, Mittal S, Prakash A, Satsangi S, Mahto PK, Swain BP. Synthesis and characterization of Fe_3O_4 nanoparticles for nanofluid applications: a review. IOP Conf Series Mater Sci Eng. 2018;377:012187.
26. Pathak S, Verma R, Singhal S, Chaturvedi R, Kumar P, Sharma P, et al. Spin dynamics investigations of multifunctional ambient scalable Fe_3O_4 surface decorated ZnO magnetic nanocomposite using FMR. Sci Rep. 2021;11(1):3799.
27. Marcos-Hernández M, Cerrón-Calle GA, Ge Y, Garcia-Segura S, Sánchez-Sánchez CM, Fajardo AS, et al. Effect of Surface functionalization of Fe_3O_4 nano-enable electrodes on the electrochemical reduction of nitrate. Separ Purif Tech. 2022;282:119771.
28. Urian YA, Atoche-Medrano JJ, Quispe LT, Félix LL, Coaquira JAH. Study of the surface properties and particle-particle interactions in oleic acid-coated Fe_3O_4 nanoparticles. J Magn Magn Mater. 2021;525:167686.
29. Zhang XH, Zhu JL, Ban YP, Liu FG, Jin LJ, Hu HQ. Effect of Fe_2O_3 on the pyrolysis of two demineralized coal using in-situ pyrolysis photoionization time-of-flight mass spectrometry. J Fuel Chem Technol. 2021;49(5):589-97.
30. Orbulet OD, Borda C, Garleanu D, Garleanu G, Stancu A, Modrogan C. Fe_3O_4 particles functionalized with EDTA and PVA: preparation, characterization and their use in removal of manganese ions from synthetic aqueous solutions. UPB Sci Bull Ser B. Chem Mater Sci. 2021;83:101-16.
31. Kushwaha P, Chauhan P. Synthesis of spherical and Rod-Like EDTA assisted α-Fe_2O_3 nanoparticles via Co-precipitation method. Mater Today Proc. 2021;44(2):3086-90.
32. Sanders JP, Gallager PK. Kinetics of the oxidation of magnetite using simultaneous TG/DSC. J Therm Anal Calorim. 2003;72:777-89.
33. McCarty KF, Monti M, Nie S, Siegel DA, Starodub E, El Gabaly F, et al. Oxidation of magnetite (100) to hematite observed by in situ spectroscopy and microscopy. J Phys Chem C. 2014;118(34):19768-77.
34. Nie S, Starodub E, Monti M, Siegel DA, Vergara L, El Gabaly F, et al. Insight into magnetite's redox catalysis from observing surface morphology during oxidation. J Am Chem Soc. 2013;135(27):10091-8.
35. Sardari A, Alamdari EK, Noaparast M, Shafaei SS. Kinetics of magnetite oxidation under non-isothermal conditions. Int J Miner Metall Mater. 2017;24(5):486-92.
36. Sanders JP, Gallager PK. Thermogravimetric evidence of γ- Fe2O3 as an intermediate in the oxidation of magnetite. Thermochim Acta. 2003;406:241-3.
37. Salmani M, Alamdari EK, Firoozi S. Isoconversional analysis of thermal dissociation kinetics of hematite in air inert atmospheres. J Therm Anal Calorim. 2017;128:1385-90.
38. Moura A, Gaglieri C, Alarcon RT, Ferreira PO, Magdalena AG, Bannach G. Non-isothermal kinetic study of andiroba and babassu oils. Braz J Therm Anal. 2017;6(4):2-11.
39. Alarcon RT, Gaglieri C, Caires FJ, Magdalena AG, Castro RAE, Bannach G. Thermoanalytical study of sweetener myo-inositol: α and β polymorphs. Food Chem. 2017;237:1149-54.
40. Silva JEE, Alarcon RT, Gaglieri C, Magdalena AG, Silva-Filho LC, Bannach G. New thermal study of polymerization kinetics of methylene diphenyl diisocyanate. J Therm Anal Calorim. 2018;133(3):1455-62.
41. Pires OAB, Alarcon RT, Gaglieri C, Silva-Filho LC, Bannach G. Synthesis and characterization of a biopolymer of glycerol and macadamia oil. J Therm Anal Calorim. 2018;137(1):161-70.
42. Holanda BBC, Alarcon RT, Gaglieri C, Souza AR, Castro RAE, Rosa PCP, et al. Thermal studies, degradation kinetics, equilibrium solubility, DFT, MIR and XRPD analyses of a new cocrystal of gemfibrozil and isonicotinamide. J Therm Anal Calorim. 2019;136(5):2049-62.
43. Vyazovkin S, Burnham AK, Criado JM, Pérez-Maqueda LA, Popescu C, Sbirrazzuoli N. ICTAC Kinetics Committee recommendations for performing kinetic computations on thermal analysis data. Thermochim Acta. 2011;520(1-2):1-19.
44. Netzsch. Thermokinetics [Internet]. 2022 [cited 2022 June 22]. Available from: https://kinetics.netzsch.com/en/
45. Friedman HL. Kinetics of thermal degradation of char-forming plastics from thermogravimetry. Application to a phenolic plastic. J Polym Sci Part C Polym Symp. 1964;6(1):183-95.
46. Yur'ev BP, Goltsev VA. Oxidation of magnetite. Steel Transl. 2016;46:735-9.
47. Colombo U, Gazzarrini F, Lanzavecchia G, Sironi G. Magnetite oxidation: a proposed mechanism. Science. 1965;147(3661):1033.
48. Wendlant WW. Thermal analysis. 3rd ed. New York: Wiley-Interscience; 1986.